Fracture energy based constitutive models for tensile fracture of metal powder compacts

P. Jonsén *, H.-Å. Häggblad

Department of Applied Physics and Mechanical Engineering, Luleå University of Technology, SE-971 87 Luleå, Sweden

Abstract

Diametral compression test or the Brazilian disc test is commonly used to characterise the tensile strength of brittle materials. A general fracture model based on energy assumptions is proposed for simulation of the discrete and localised tensile fracturing process in metal powder. The characteristics of the tensile fracture development of the central crack in diametral tested specimen is numerically studied. The softening rate of the model is obtained from the corresponding rate of the dissipated energy. Finite element simulations of the diametral compression test are performed with the proposed tensile fracture model used in conjunction with a Cap model for the deformation of the powder material. The results agree reasonably with experiments.

© 2007 Elsevier Ltd. All rights reserved.

Keywords: Powder mechanics; Green bodies; Fracture energy; Tensile crack; Fracture model; Finite element analysis; Cohesive zone

1. Introduction

A common process in powder metallurgy (PM) is cold uniaxial compaction with rigid tools and die. The main stages in the pressing process are powder fill and transfer, compaction, axial load release, ejection, release from the die, post-ejection and handling. Cracks can be initiated during all stages, but are primarily formed during compaction, ejection and handling. Fracture in powder compacts can be defined as separation or fragmentation of a solid body into two or more parts, under the action of stress and is the result of crack initiation and propagation. According to Zenger and Cai (1997), cracks in a green PM compact during powder pressing are characterised by broken inter-particle bonds and/or never formed inter-particle bonds during compaction. The main cause of broken inter-particle bonds is the pulling apart of powder particles which have been mechanically locked during compaction. The pulling apart of powder particles is caused by tensile forces, lateral shear forces, or a combination of these two. Prediction of shear crack formation using a softening material

---

* Corresponding author. Tel.: +46 920 491160; fax: +46 920 491047.
  E-mail address: Par.Jonsen@ltu.se (P. Jonsén).

law for powder pressing have been performed in Coube (1998). A mesh size independent smeared crack approach using a fracture energy dependent softening modulus is proposed in Oliver et al. (2005).

The diametral compression test, also called the Brazilian disc test, is considered to be a reliable and accurate method to determine strength of brittle and low strength material, see Fairhurst (1964) and Hondros (1959). The test has been used to measure the tensile strength of concrete, rock, coal, polymers, cemented carbides, and ceramics. For powder material no extensive machining of specialised shape is needed as a powder material can be pressed directly to a desired geometry. During the test a thin disc is compressed to failure across a diameter. The compression induces tensile stresses, normal to the compressed diameter, which are constant over a region around the centre of the disc. In Jonsén (2006), the fracturing process during diametral compression test is characterised for water atomised metal powder. The main results are tensile strength and fracture energy as functions of density.

Powder material is pressure sensitive and density dependent which induces a complex material behaviour. To numerically reproduce this behaviour the choice of constitutive model is critical. A better understanding of the material behaviour will give advantages to other production methods and allow more extensive computer simulations. Numerical analysis of tool kinematics, tool force, tool stresses, tool design, density distribution, green strength, residual stresses and crack initiation etc. might reduce today's time consuming trial and error methods.

The aim of this work is to model tensile cracking and crack propagation in metal powder compacts during loading. Here, the deformation and the fracturing is separately modelled. An elastic–plastic model for the deformation of the powder material. As fracturing is a discrete and local process the fracture is modelled with an cohesive zone model. The form of the cohesive law have been evaluated. Finite element simulations of the fracture process are performed and compared with experimental tests.

2. Fracture process in diametral compression tests

In Jonsén (2006) diametral compression tests are performed for an iron based metal powder with a density range of 4.90–7.35 g/cm^3. The samples was 25 mm in diameter with a thickness of 5 and 10 mm. To avoid fracture at the loading point the load was distributed over a small arc. The load versus displacement response in the diametral compression tests is shown in Fig. 1 from Jonsén (2006).

The load response of the test is described in several stages, see Figs. 1 and 2. Stage 1 illustrates the initial nonlinear elastic load–displacement relation. In stage 2, from point A, the powder shows a linear elastic relationship. In stage 3, the response diverges from the linear as a crack is initiated at B. The crack propagates moderately through the sample and the load reaches maximum at C. In stage 4, the unstable crack growth
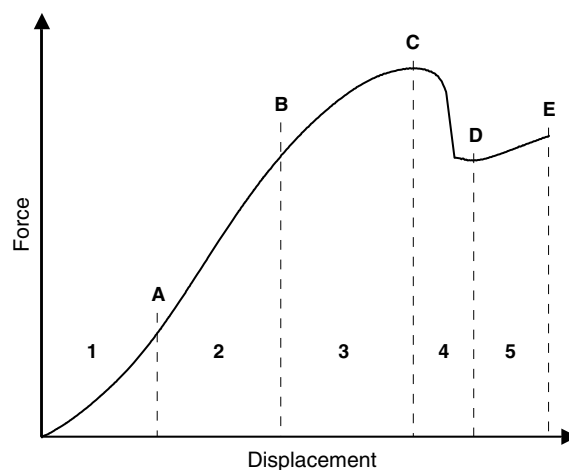

Fig. 1. A typical force–displacement curve for a diametral test, from Jonsén (2006). 1 – nonlinear elastic, 2 – linear elastic, 3 – stable crack extension, 4 – 'unstable' crack extension, 5 – stable loading of two halves.

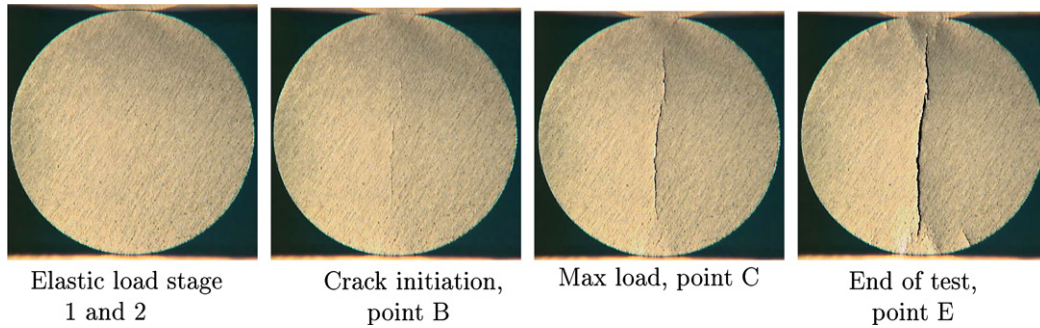| Elastic load stage 1 and 2 | Crack initiation, point B | Max load, point C | End of test, point E |

Fig. 2. Crack development during the test, from Jonsén (2006). The pictures are related to different positions on the load curve in Fig. 1.

stage, the load decreases rapidly as the crack is widened. In stage 5, from point D, the load increases again and the behaviour corresponds to the loading of two separate disc halves. The end of test is reached at E. Close to the loaded edge of the disc, shear band and small tensile cracks appear. The decreasing load is caused by tensile cracking which is a local and discrete process driven by cohesive stresses. Timoshenko and Goodier (1970) postulated a theoretical basis for the stress state of a circular disc subjected to two concentrated diametral forces assuming plane stress. In the centre of the disc the stress can be described with the following relation:

$$\sigma_x = \frac{2P}{\pi D t} \tag{1}$$

$$\sigma_y = -\frac{6P}{\pi D t} \tag{2}$$

where P is applied load, t thickness of the disc, D diameter, σ_x and σ_y normal stresses in the directions perpendicular and parallel to the loaded diameter. Tensile strength is calculated at point B using Eq. (1). Hondros (1959) presented a theory for the case of a pressure applied over two diametrically opposite arcs. He also showed that this theory agrees with Eqs. (1) and (2) in the centre of the disc. Fahad (1996) performed a finite element analysis of both arc and point loading and showed that a good correlation exists between the solutions for arc angles up to at least 22.90° for stresses in the centre of the disk.

3. Plasticity model

The constitutive behaviour of the powder material is governed by a Cap model presented in Jonsén and Häggblad (2005a). To control yielding the model consists of a density dependent perfectly plastic failure envelope and a hardening cap, see Fig. 3. The model is fitted to experimental data for the actual powder. Plastic deformation follows an associative flow rule and in the principal stress space the yield functions are given by
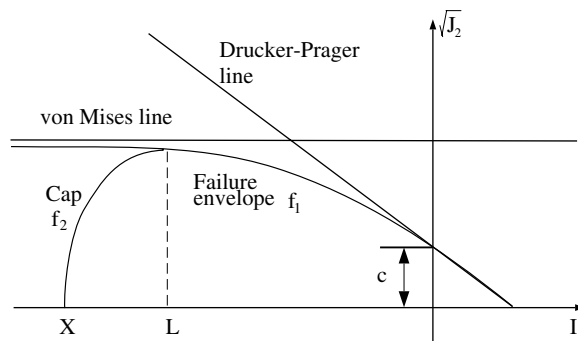

Fig. 3. The Cap model for powder material in principal stress space $I_1 - \sqrt{J_2}$. f_1 is the failure envelope, f_2 is the moving strain hardening cap and c is the cohesion.

$$f_1(I_1, J_2) = \sqrt{J_2} - [\alpha - (a_1 - \exp(a_2(\rho)^{a_3}))\gamma \exp(\beta I_1) - \theta I_1] = 0 \tag{3}$$

$$f_2(I_1, J_2, \kappa) = \sqrt{J_2} - \frac{1}{R}\sqrt{(X-L)^2 - (I_1-L)^2} = 0 \tag{4}$$

where I_1 is the first invariant of the stress tensor and J_2 is the second invariant of the deviatoric stress tensor. The parameter κ is an internal state hardening variable and a function of the plastic volumetric strain ε_v^p and ρ is the relative density. L is the point of intersection between the two yield surfaces and X the point of intersection between the hydrostatic axis and the cap function. The parameter R, which is the ratio between the horizontal and vertical ellipse axes, defines the shape of the cap in the $I_1 - \sqrt{J_2}$ plane and α, β, γ, θ, a_1, a_2 and a_3 are material parameters.

4. Fracture material models

Linear elastic fracture mechanics is not applicable to cracking in metal powder compacts because the fracture zone is large compared to the crack dimension. Hillerborg et al. (1976) proposed a nonlinear fracture model suited for numerical analysis of crack propagation in concrete. This crack model uses ideas from the Barenblatt (1962) theory, in which cohesive forces act on the crack planes and decrease when a crack is widening. Barenblatt proved the existence of cohesive forces acting on the crack surfaces and that the opposite faces of a crack close smoothly at the tip of the cohesive zone, see Fig. 4.

The present crack model is an extension of the Barenblatt's cohesive force model to nonlinear fracture mechanics where the forces are due to macroscopic effects from microcracking in the fracture zone. The numerical implementation uses a discrete crack model, where the forces between the nodes in the fictitious crack follows an assumed stress crack–width relation. See Fig. 5 for an illustration of the crack model in finite element analysis. A fracture material model with a linear stress crack–width relation Hillerborg et al. (1976) is

$$\sigma_n(w) = \sigma_f\left(1 - \frac{w}{w_c}\right) \tag{5}$$

where σ_n is the tensile stress normal to the crackplane, σ_f is the tensile strength, w is the crack–width and w_c is the critical crack–width, see Fig. 6. This model was applied by Jonsén and Häggblad (2005b) to simulate diametral compression tests of metal powder compacts.

Nilsson and Oldenburg (1983) showed in an analysis of impact loading of concrete structures that the energy dissipation in the fracture material model was essential if accurate results were to be obtained. They considered the stress crack–width relation as a softening function with the fracture energy as one parameter in the following model:
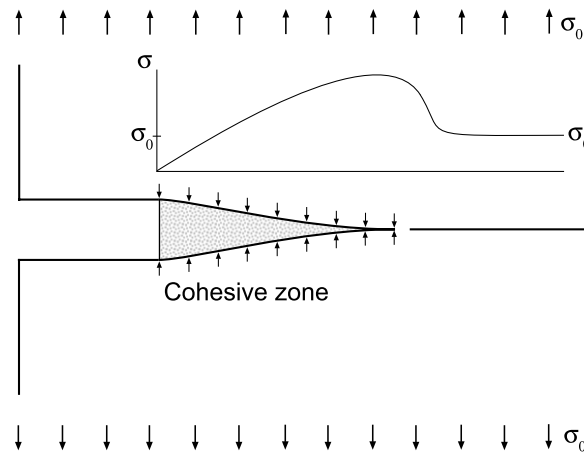

Fig. 4. The Barenblatt model with a cohesive zone ahead of the crack tip, stress distribution and crack geometry. The stress and displacement fields are finite and continuous at the crack tip.
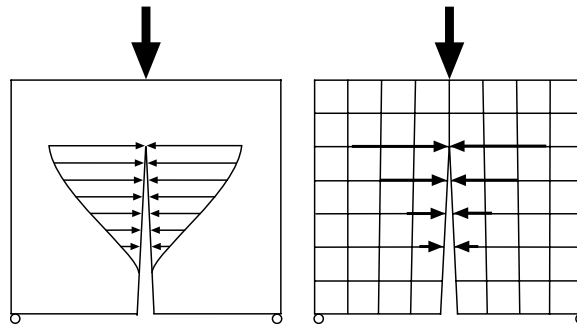
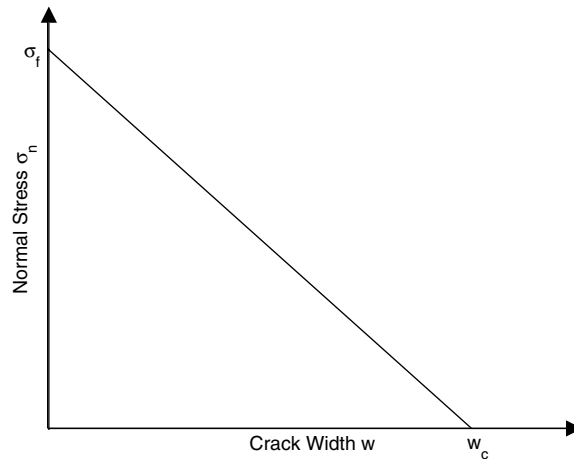Fig. 5. Illustration of the fictitious crack for finite element analysis.

Fig. 6. Fracture model with a linear stress versus crack–width relationship, from Hillerborg et al. (1976).

$$\sigma_n(w) = \sigma_f \exp\left(\frac{-\sigma_f}{G_f} w\right) \tag{6}$$

where the energy required to fully open a crack of unit area G_f is defined as

$$G_f = \int_0^\infty \sigma_n(w)\, \mathrm{d}w \tag{7}$$

Experimental observation in Jonsén (2006) shows that tensile cracking in pressed metal powder is a discrete and localised phenomenon exhibiting a softening effect caused by decreasing cohesive stresses. A density dependent fracture model with a potential function is proposed for metal powder applications. Below is the model shown in its general form

$$\sigma_n(w) = \frac{\sigma_f(\rho)}{1 + (k(\rho)w)^l} \qquad \text{with } l \in \mathbb{R}(1, \infty) \tag{8}$$

where w is the crack opening, $\sigma_f(\rho)$ tensile strength as function of density and σ_n normal stress for a crack opening normal to the crack plane. The model has been studied for different values of the exponent l. For a general case the evaluation of the parameter $k(\rho)$ is given by Eqs. (7) and (8) as

$$G_f(\rho) = \sigma_f(\rho) \int_0^\infty \frac{\mathrm{d}w}{1 + (k(\rho)w)^l} = \frac{\pi}{l \sin(\frac{\pi}{l})} \frac{\sigma_f(\rho)}{k(\rho)} \tag{9}$$
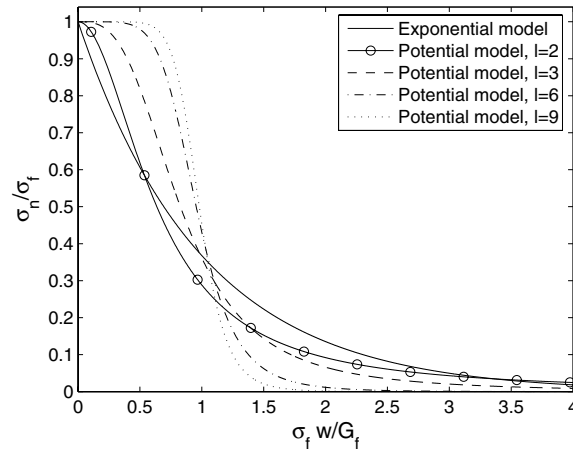
and for the general case $k(\rho)$ becomes

Fig. 7. The exponential and the potential function models used in the numerical investigation.

$$k(\rho) = \frac{\pi}{l\sin(\frac{\pi}{l})} \frac{\sigma_f(\rho)}{G_f(\rho)} \tag{10}$$

For $l = 2.0$ the stress σ_n becomes

$$\sigma_n(w) = \frac{\sigma_f(\rho)}{1 + \left(\frac{\pi}{2} \frac{\sigma_f(\rho)}{G_f(\rho)} w\right)^{2.0}} \tag{11}$$

and for $l = 3.0$ this stress becomes

$$\sigma_n(w) = \frac{\sigma_f(\rho)}{1 + \left(\frac{2\sqrt{3}\pi}{9} \frac{\sigma_f(\rho)}{G_f(\rho)} w\right)^{3.0}} \tag{12}$$

In Fig. 7 the exponential model Eq. (6) and the proposed fracture model Eq. (8) with different values of l are shown. By varying the exponent l the characteristics of σ_n can be affected. For a low value of l, the σ_n-function decreases moderately from the beginning to the end of the fracture process. With a large value of l, the σ_n-function is almost constant at the onset of fracture, but decreases rapidly as the function has a larger slope. Another feature of the potential function is that the derivative of the normal stress as function of the crack–width is zero for $w = 0$, see Eq. (13).

$$\lim_{w \to 0} \frac{d\sigma_n(w)}{dw} = \lim_{w \to 0} -\frac{\sigma_f(\rho)lk(\rho)^l w^{l-1}}{(1 + (k(\rho)w)^l)^2} = -\frac{0}{1+0} = 0 \tag{13}$$

5. Finite element simulation of diametral compression

Diametral compression tests of pressed powder discs are virtually reproduced, validated and compared with experimental results. A three-dimensional finite element model of the tool and the disc where the material response of the powder is controlled with a Cap model is exploited in the simulations. A fracture model controls the fictitious crack with a stress crack–width relation. The force displacement response for different stress crack–width relations at equivalent G_f are studied. In the comparison with experiments two different densities 5.65 and 7.21 g/cm^3 are studied. In the experimental study by Jonsén (2006) 25 mm diameter samples with 5 and 10 mm thickness are exploited and here only $t = 5$ mm samples are reproduced. In Fig. 8 the symmetric finite element mesh used in the numerical analysis containing 20 666 nodes and 17 234 brick elements is shown.

The tool is considered rigid and a small finite arc with radius 12.7 mm and an angular width of 14.0° distributes the load to the sample as in the experiments. Friction between the tool and the disc is assumed
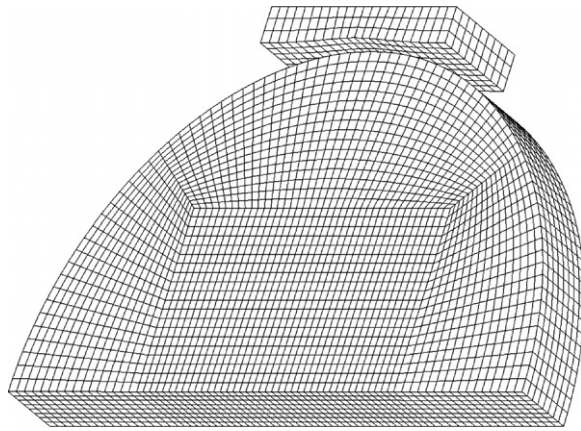
Fig. 8. The symmetric finite element mesh used for simulations of diametral compression test of pressed powder.

constant and set to $\mu = 0.10$. Symmetry condition is exploited to facilitate computing. Only the upper half of the disc and half its thickness is modelled. A third symmetry plane located in the middle of the disc is exploited to model the fracturing. Between the two halves of powder a tiebreak contact is active for nodes which initially are in contact. The stress is limited by a yield condition σ_f and fracturing is a function of the crack–width opening controlled by the fracture models proposed above.

5.1. Validation of the numerical model

A validation of the numerical model has been carried out. In this validation the proposed fracture model Eq. (8) for $l = 3$ controls the fracturing which is governed by a stress crack–width relation. The force response, crack–width, crack length and dissipated energy are checked. In Jonsén (2006) a method to estimate the dissipated part of the energy W from the total energy consumed in the test is proposed. This method is also used to check the numerical model. Three different simulations are performed for the density 7.21 g/cm^3. In the first simulation, V1, a fracture energy of $G_f = 1489$ J/m^2 is used, in the second simulation, V2, fracture energy $G_f = 1638$ J/m^2, which is a 10% increase compared to V1. For V1 and V2, the tensile strength is 16.0 MPa. The tensile strength, $\sigma_f = 16.0$ MPa, corresponds to the force at point B in Fig. 1 using Eq. (1). To separate the dissipated energy from the fracturing of the central crack and the total consumed energy a simulation of two separate halves is performed in the third simulation, V3. The fracture model is removed and the response is from loading of two separate halves with $\sigma_f = 0$. In Fig. 9 the horizontal stress σ_x distribution is shown for simulation V1 in the elastic range before crack initiation and at the maximum load point.
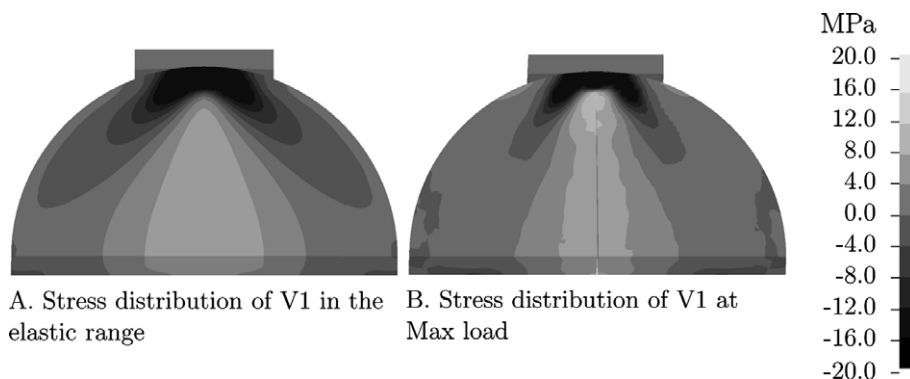

A. Stress distribution of V1 in the elastic range

B. Stress distribution of V1 at Max load

Fig. 9. The horizontal stress, σ_x, distribution for simulation V1 in the elastic range and at maximum load. At the maximum load the central crack is partly opened.

In Fig. 10 the global response from the virtual diametral compression tests V1, V2 and V3 is shown. The response curves from V1 and V3 intersects in the point marked (∗1) and the area enclosed by V1 and V3 is defined as the dissipated energy W. The intersection point between V1 and V2 is marked (∗2) in Fig. 10 and the area enclosed by V1 and V2 is ΔW the difference in dissipated energy between V1 and V2. Dissipated energy from V1 is $W = 0.1344$ J and $\Delta W = 0.0145$ J which gives $\Delta W/W = 0.108$.

Another approach to determine the dissipated energy is to calculate the energy consumed in the fracture interface. Dissipated energy W can be calculated incrementally from time n to time $n + 1$ from the fracture interface as

$$W^{n+1} = W^n + \left[\sum_{i=1}^{nsn} \Delta F_i^{\text{slave}} \times \Delta d_i^{\text{slave}} + \sum_{i=1}^{nmn} \Delta F_i^{\text{master}} \times \Delta d_i^{\text{master}} \right] \tag{14}$$

Where W^n is the stored energy, nsn is the number of slave nodes, nmn is the number of master nodes, $\Delta F_i^{\text{slave}}$ is the interface force between the i-th slave node and the contact segment, $\Delta F_i^{\text{master}}$ is the interface force between the i-th master node and the contact segment, $\Delta d_i^{\text{slave}}$ is the incremental distance the i-th slave node has moved during the current time step and $\Delta d_i^{\text{master}}$ is the incremental distance the i-th slave node has moved during the current time step. In Fig. 11 dissipated energy as a function of tool displacement for the central crack in sim-
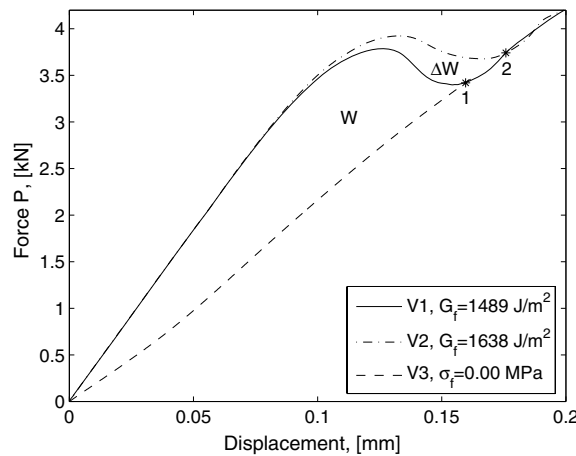

Fig. 10. Force vs. displacement response from simulation V1 with fracture energy G_f is compared with simulation V2 with $1.10 G_f$. Simulation V3, loading of two separate halves $\sigma_f = 0.0$ is also shown. The area enclosed by simulation V1 and V3 is the dissipated energy W, intersection points between simulation V1 and V3 is marked (∗1) and between V1 and V2 is marked (∗2).
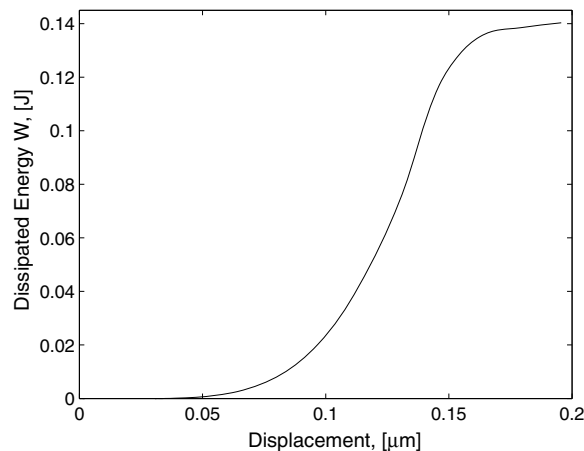

Fig. 11. Dissipated energy W calculated with Eq. (14) as a function of tool displacement for the central crack in simulation V1.

Table 1
Validation of dissipated energy W for the fracture simulations V1 and V2

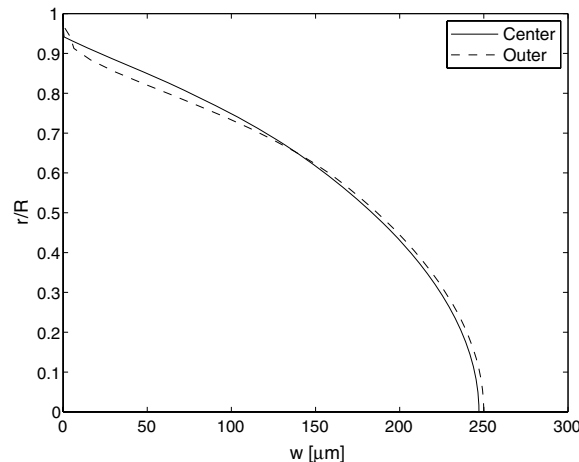| Method	V1 W (J)	V2 W (J)	Difference $\Delta W/W$ (%)
Global force estimation	0.1344	0.1489	10.8
Fracture interface	0.1339	0.1473	10.0

Fig. 12. Central crack form in the centre of the crack surface and outer edge at (∗1) in Fig. 10.

ulation V1 is shown. The dissipated energy W is calculated with this method for V1 at (∗1) and V2 at (∗2), see Fig. 10. The results from dissipated energy calculations using the global load response method from Jonsén (2006) and the contact interface method Eq. (14) are shown in Table 1. Both methods give almost equal result of the dissipated energy for V1 and V2. The table shows also that the 10% increase in G_f gives an equal increase in W. This is correct as the crack surface area A_f of V1 at (∗1) and V2 at (∗2) are nearly equal.

Before crack initiation around 80% of the vertical diameter is loaded in tension horizontally. During fracturing stresses are controlled and related to crack–width w by the fracture model. As the crack opens up tensile stresses will decrease around the centre of the disc and be more concentrated where the crack is less opened. The crack–width is checked at the intersection point between simulation V1 and V3, (∗1), see Fig. 10. At the crack tip most of the energy is left and to numerically determine the crack length and relate it to a real value can be difficult. In Fig. 12 crack length against crack–width on the outer edge and centre of the crack surface at (∗1) is shown. The maximum crack–width is 250 μm and the crack length is around 90% of the vertical radius at the end of the test. Of course this value depends on the tolerance that is used in the determination of the crack length.

5.2. Results

The load response from the finite element model with a fictitious crack is studied for different fracture models. All models have equal G_f, but different functions for the stress versus crack–width relation. Input data to the numerical model is taken from the experimental investigation carried out in Jonsén (2006). Using equal input data as for the validation simulation V1, the density of the powder is $\rho = 7.21$ g/cm^3, the fracture energy, $G_f = 1489$ J/m^2 and the tensile strength, $\sigma_f = 16.0$ MPa for all fracture models. In Fig. 13 force versus displacement for the exponential model by Nilsson and Oldenburg Eq. (6) and the suggested potential model Eq. (8) with $l = 2$, 3 and 9 are shown. In Table 2 the maximum and minimum loads with corresponding displacements from Fig. 13 are shown. A high value of l gives a larger difference in the maximum and minimum load values of the response curve after fracture. The exponential model have least difference in between maximum and minimum followed by the potential function model with $l = 2$. The response difference is probably due to that
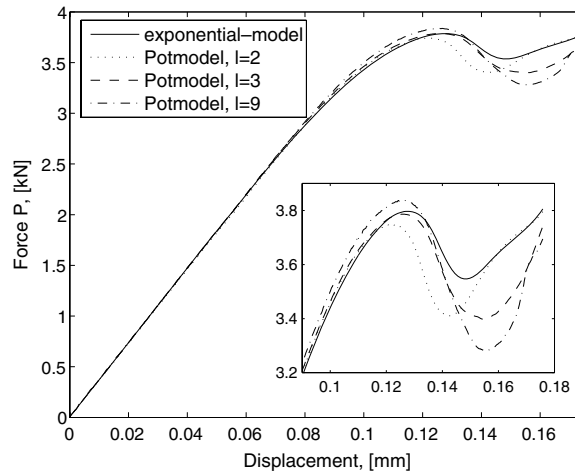
Fig. 13. Comparison between different force displacement responses for the studied fracture models.

Table 2
Maximum and minimum loads with corresponding displacement from Fig. 13

Model	Max load P (kN)	Displacement at P_{Max} (μm)	Min load P (kN)	Displacement at P_{Min} (μm)
Exponential-model	3.786	127.9	3.536	148.3
Pot-model, $l = 2$	3.743	122.4	3.403	142.0
Pot-model, $l = 3$	3.787	126.1	3.399	154.3
Pot-model, $l = 9$	3.838	125.7	3.281	155.4

The Exponential-model is the model proposed by Nilsson and Oldenburg Eq. (6) and Pot-model is the suggested potential function model Eq. (8).

a low value of l will have more energy left at high w values. On the other hand a high value of l will stiffen the response as more energy is needed to open the crack at the beginning of the fracturing.

From the experimental work carried out by Jonsén (2006) two specific experiments are compared to finite element simulations. In the first experiment the measured fracture energy is $G_f = 1489$ J/m^2 with a tensile strength $\sigma_f = 16.0$ MPa at the density $\rho = 7.21$ g/cm^3, the second experimental test is carried out at the density $\rho = 5.65$ g/cm^3 and the measured fracture energy is $G_f = 112$ J/m^2 with a tensile strength $\sigma_f = 1.28$ MPa. The proposed fracture model with $l = 3$ and $l = 9$ is used for both densities. In Fig. 14 the load responses from the
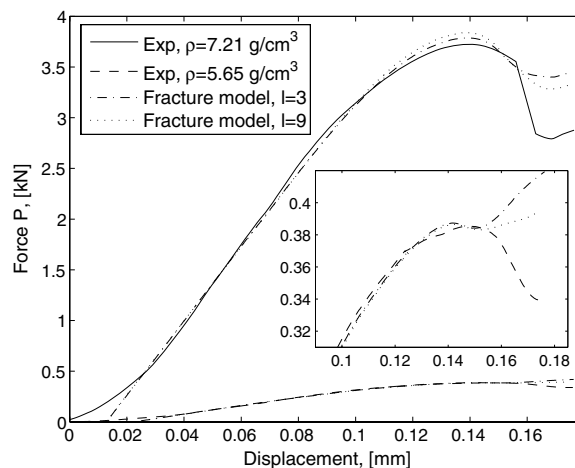

Fig. 14. Comparison between experimental response and finite element simulations with the proposed fracture model for $l = 3$ and 9 at the densities 7.21 and 5.65 g/cm^3. The load response for the density 5.65 g/cm^3 around the maximum load is shown in the magnified plot.

experimental and finite element simulations are shown for both densities. The constitutive model for the powder does not include the nonlinear elastic behaviour shown experimentally in the initial loading stage, stage 1 in Fig. 1. This nonlinear effect arises from the geometrical nonlinearity of the contact problem between the powder particles. The nonlinear contributions are added to the displacements of the numerical simulations in the figures so that the numerical results start at a nonzero displacement value.

5.2.1. Cut off parameter w_c

According to the experimental study in Jonsén (2006), unstable crack widening occurs after the maximum load, see stage 4 Fig. 1. This is not shown in the simulated response above. Another difference between the force displacement response from experimental tests and numerical simulation is that the minimum value after fraction is lower in the real test then for simulated ones. The suggested model Eq. (8) is defined for $0 \leqslant w < \infty$ which is unrealistic. One difference may be that there is energy left in the simulated crack even at the end of the test. In the fracture model proposed by Hillerborg et al. Eq. (5) the fracture model works on a finite interval $0 \leqslant w < w_c$ where w_c is a critical crack–width. By introducing w_c as a cut off parameter into the suggested model Eq. (8) the model will be switched of at a certain crack-width and the stress $\sigma_n = 0$ for $w > w_c$.

In Fig. 15 the suggested model Eq. (8) with $l = 3$ and with w_c as a cut of parameter is shown. The grey area in Fig. 15 is the omitted fracture energy. The approach to turn off the fracture model at a critical crack–width, violates the theory described above as G_f is a physical parameter and a cut off may decrease the value of G_f, see Eq. (7). The stress versus crack–width relation can be compensated so that the area below the function still represents G_f. In the comparison with experimental load response a fracture model with $l = 3$ is used, see Fig. 14. Below is an example where the cut off parameter w_c is included in the same model. The particle size of the powder mix is 20–180 μm and the roughness of the fracture surface is estimated to 100–200 μm in Jonsén (2006). The value of the critical crack–width, w_c is set to 150 μm and this reduces the fracture energy G_f to 1350 J/m² which is about 10% lower than the original G_f. In this simulation this change in G_f is not compensated for. To compare the effect of the cut off parameter w_c an equal fracture model with no cut off parameter ($G_f = 1489$ J/m²) is used in the reference simulation. In Fig. 16 the response from finite element simulations using $w_c = 150$ μm is shown together with the load response from the reference simulation and the experimental test. The response from the extended model including w_c improves the load response for the model compared to the experimental response, see Figs. 14 and 16. In Table 3 the maximum and minimum loads with corresponding displacement and dissipated energies for experimental and simulated diametral compression tests with and without cut off parameter w_c are presented.

Experimental dissipated energy (∗) from Jonsén (2006) is evaluated with a global method and the simulated energy is calculated with Eq. (14). With the critical crack–width, w_c included as a parameter the maximum load response is unchanged, but the minimum load is changed. Comparison of dissipated energy in Table 3
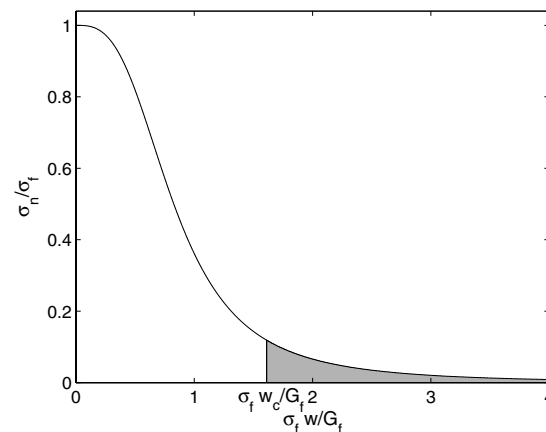

Fig. 15. Fracture model with extended with a critical crack opening width w_c. The stress $\sigma_n = 0$ for $w > w_c$ and the grey area is the cancelled fracture energy.
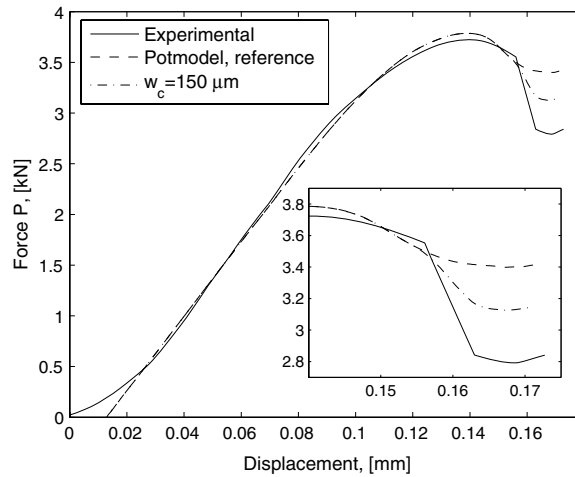
Fig. 16. Load response from the potential function model $l = 3$ with and without cut off value $w_c = 150$ μm compared with an experimental diametral compression test.

Table 3
Load response from an experimental diametral compression test and the potential function model $l = 3$, with and without cut off parameter

	Max P (kN)	Displacement at P_{Max} (μm)	Min P (kN)	Displacement at P_{Min} (μm)	Dissipated Energy W (J)
Experiment	3.724	140.0	2.792	168.6	0.1489 (∗)
Pot-model, ref	3.787	139.1	3.399	167.3	0.1339 (∗1)
$w_c = 150$ μm	3.787	139.1	3.126	167.3	0.1313 (∗1)

Experimental dissipated energy W from Jonsén (2006) (∗) estimated with a global method. Dissipated energy W at equal displacement (∗1) from Fig. 10.

for the simulation with a cut off value and the reference simulation shows that a critical crack–width of $w_c = 150$ μm gives a 1.9% lower value of the dissipated energy compared to a the reference simulation.

6. Discussion and conclusion

The diametral compression test is an established method for measurement of tensile strength in brittle materials such as rock, concrete, polymers, ceramics etc. During testing a load P, applied along a diameter, induces compressive stresses. Stresses are tensile perpendicular to the compressed diameter. These tensile stresses act until failure. Pressed and unsintered powder compacts are low strength material and the diametral compression test is an alternative method as an ordinary tensile test is almost impossible to perform and results are given with a large uncertainty, see Dorémus et al. (2001).

An energy dependent fracture model Eq. (8) together with Eq. (10) to control dissipated energy for pressed powder is suggested in this work. A property of the potential function is that the derivative of the normal stress as function of the crack–width is zero for $w = 0$, see Eq. (13). This grants function stability at the onset of fracture. The numerical modelling of fracture in pressed powder is based on an experimental investigation of the diametral compression test performed for pressed water atomised metal powder in Jonsén (2006). One of the main findings from the experimental work is that pressed powder seems to exhibit a cohesive behaviour upon tensile loading. Experimentally determined tensile strength σ_f and fracture energy G_f as functions of density are also results from the study, see Jonsén (2006).

Finite element simulations of diametrically compressed discs with a fictitious crack controlled by a stress versus crack-width relationship are performed in this work. In the simulation tensile strength σ_f is used as failure condition and limits the stress in the fracture interface. After crack initiation, damage is governed with the

energy dependent fracture model. A validation using two different methods to calculate dissipated energy is performed. Both methods show almost equal result regarding the dissipated energy. The difference between the methods is that the global method includes plastic and elastic energy from the material and the fracture interface method only includes the energy in the interface, work dissipated in decohesion. The validation shows that an increase in the parameter G_f results in an almost equally corresponding increase of dissipated energy W, see Table 1. This shows that the major part of the dissipated energy is from the work dissipated in decohesion.

The form of the stress versus crack–width relation governs dissipation of crack surface energy and thereby affects the load response, see Fig. 13 and Table 2. The difference between the maximum and minimum load value after fracture increases with the exponent l. The response difference is due to dissipation of energy. A small value of l will have more energy left at large w compared to models with larger values of l. On the other hand a large value of l will stiffen the load response at the beginning of the fracture process as most of the energy is consumed early in the fracturing. In comparison with experiments the proposed model Eq. (8) using $l = 3$ shows a fair agreement with the maximum load while $l = 9$ gives a larger maximum load. Both models gives too high values of the minimum load compared to experiments, but $l = 9$ gives a smaller value than $l = 3$, see Fig. 14.

A modification of the proposed model is also considered and here the fracture model works on a finite interval $0 \leqslant w < w_c$ where the critical crack–width w_c is introduced as a cut off parameter, see Fig. 15. Using the suggested model it is important not to omit too much energy as it affects the fracture energy G_f, which will be reduced. If the cut off parameter is used in the model the omitted energy should be compensated so that G_f is unchanged. The extended model improves the simulated load response, the maximum load is unchanged, but the minimum load after fracture is changed, see Table 3 and Fig. 16. Using w_c in fracture modelling has a disadvantage as the critical crack–width might be difficult to determine.

The simulation results show that it is possible to simulate fracturing of pressed powder. The global method to estimate the dissipated energy W and the fracture energy G_f from a real test seems to be a good approximation. From experiments Jonsén (2006) the length of the central crack is estimated to be fully open 80% of the disc diameter. In the numerical simulation the crack length is around 90% of the disc diameter at the end of the simulation, but it is only partly opened, see Fig. 12. Thus, the assumption of a crack length of 80% for the determination of G_f is reasonably correct when comparing with the simulations. In the simulated result only the fracturing of the central crack is modelled. This gives a higher final stiffness than for a real test where shear bands and other types of fracture appear. One possibility would be to include effects of shear cracking in the modelling, see Dahlblom and Ottosen (1990).

Acknowledgement

References

Barenblatt, G.I., 1962. The mathematical theory of equilibrium cracks in brittle fracture. Adv. Appl. Mech. 7, 55–129.

Coube, O., March 1998. Modelling and numerical simulation of powder die compaction with consideration of cracking. PhD thesis, Fraunhofer Institute Werkstoffmechanik.

Dahlblom, O., Ottosen, N.S., 1990. Smeared crack analysis using generalized fictitious crack model. J. Eng. Mech. 116 (1), 55–76.

Dorémus, P., Toussaint, F., Alvin, O., 2001. Simple test standard procedure for the characterisation of green compacted powder. In: Zavaliangos, A., Laptev, A. (Eds.), Computer and Systems Science, vol. 176 of III. NATO, IOS Press, Amsterdam, pp. 29–41.

Fahad, M.K., 1996. Stresses and failure in the diametral compression test. J. Mater. Sci. 31, 3723–3729.

Fairhurst, C., 1964. On the validity of the 'Brazilian' test for brittle material. Int. J. Rock Mech. Mining Sci. 1, 535–546.

Hillerborg, A., Modéer, M., Petersson, P.-E., 1976. Analysis of crack formation and crack growth in concrete by means of fracture mechanics and finite elements. Cement Concrete Res. 6 (6), 773–782.

Hondros, G., 1959. The evaluation of poisson's ratio and the modulus materials of a low tensile resistance by the Brazilian (indirect tensile) test with particular reference to concrete. Aust. J. Appl. Sci. 10 (3), 243–268.

Jonsén, P., 2006. Fracture and stress in powder compacts. PhD thesis, Division of Solid Mechanics, Luleå University of Technology, ISSN: 1402-1544, ISRN: LTU-DT-06/29-SE.

Jonsén, P., Häggblad, H.-Å., 2005a. Modelling and numerical investigation of the residual stress state in a green metal powder body. Powder Technol. 155 (3), 196–208.

Jonsén, P., Häggblad, H.-Å., October 2005b. Tensile fracturing in diametral compression. In: Proceedings of the 2005 European Powder Metallurgy Congress, vol. 3. European Powder Metallurgy Association, EPMA, Prague, Czech Republic, pp 377–382.

Nilsson, L., Oldenburg, M., 1983. Nonlinear wave propagation in plastic fracturing materials – a constitutive modelling and finite element analysis. In: Nonlinear Deformation Waves, Tallin 1982, IUTAM, Springer, Berlin, Germany, pp 209–217.

Oliver, J., Cante, J.C., Hernández, J.A., 2005. A numerical procedure for modeling crack formation in powder compaction based manufacturing processes. In: Ow en, D.R.J., Oñate, E., Suárez, B. (Eds.), Computational Plasticity VII, vol. 1. CIMNE, Barcelona, Spain, pp. 287–290.

Timoshenko, S.P., Goodier, J.N., 1970. Theory of Elasticity, third ed. McGraw-Hill, New York.

Zenger, D.C., Cai, H., 1997. Handbook of: The Common Cracks in Green P/M Compacts. Metal Powder Industries Federation.